Last author copy

Submitted to Journal of Guidance, Control and Dynamics on April 1st 2015, Accepted on July 29th 2015

Collision probability due to space debris clouds through a continuum approach

Francesca Letizia[1], Camilla Colombo[2], and Hugh G. Lewis[3]
University of Southampton, Southampton, United Kingdom, SO17 1BJ

As the debris population increases, the probability of collisions in space grows. Due to the high level of released energy, even collisions with small objects may produce thousands of fragments. Propagating the trajectories of all the objects produced by a breakup could be computationally expensive. Therefore, in this work debris clouds are modeled as a fluid, whose spatial density varies with time under the effect of atmospheric drag. By introducing some simplifying assumptions, such as an exponential model of the atmosphere, an analytical expression for the cloud density evolution in time is derived. The proposed approach enables the analysis of many potential fragmentation scenarios that would be time-limited with current numerical methods that rely on the integration of all the fragments' trajectories. In particular, the proposed analytical method is applied to evaluate the consequences of some recent breakups on a list of target objects. In addition, collision scenarios with different initial conditions are simulated to identify which parameters have the largest effect on the resulting collision probability. Finally, the proposed model is used to study the mutual influence among a set of high risk targets, analyzing how a fragmentation starting from one spacecraft

[1] PhD Candidate, Astronautics Research Group, f.letizia@soton.ac.uk
[2] Lecturer, PhD, Marie Curie Research fellow at Politecnico di Milano, Italy, AIAA member, c.colombo@soton.ac.uk
[3] Senior lecturer, PhD, Astronautics Research Group, h.g.lewis@soton.ac.uk

affects the collision probability of the others.

Nomenclature

A_T = target area [m^2]

a = semi-major axis [km]

e = eccentricity

err = relative error

F = fragments' flux [km^{-2}s^{-}1]

$\mathbf{f}$ = vector field

G = characteristic line of the system

H = scale height for the atmospheric model [km]

h = altitude [km]

i = inclination [rad] or [deg]

J_2 = second zonal harmonic coefficient of Earth's gravitational potential, $1.082\,62 \times 10^{-3}$

L_c = fragment characteristic length [m]

M = mean anomaly [rad] or [deg]

M_E = reference mass for collision [kg]

m_p = projectile mass [kg]

N = number of collisions

n = fragment density [-/km]

R_E = Earth's equatorial radius, $6.378\,16 \times 10^3$ km

R_H = geocentric radius of fragmentation [km]

p_c = cumulative collision probability

r = geocentric radius [km]

t = time [s]

V = volume [km^3]

v = velocity [m/s]

v_{coll} = collision velocity [km/s]

v_r = radial velocity [km/s]

v_θ = transversal velocity [km/s]

w = width of the altitude bins [km]

μ = gravitational constant, $3.986\,00 \times 10^5\,\mathrm{km^3\,s^{-2}}$

ν = true anomaly [rad] or [deg]

Ω = argument of the ascending node [rad] or [deg]

ω = argument of the periapsis [rad] or [deg]

ρ = atmospheric density [$\mathrm{kg/m^3}$]

I. Introduction

Past space missions left millions of non-operative objects in orbit and also current missions, despite mitigation measures, continue to increase the number of debris objects because, quoting Chobotov [1], 'space debris is a *self-perpetuating issue* as any new space mission generates new objects'. Currently, the focus is mostly on the largest objects of the debris population, which are the 22 000 objects larger than 10 cm that are constantly tracked from the Earth to avoid collisions with operational spacecraft [2, 3].

Objects smaller than 10 cm cannot be tracked with current radar technologies and, as a result, the contribution of small fragments to the collision probability is often neglected. Objects larger than 10 cm have also been the main scope for the evolutionary studies on the space debris population, which analyze the long term response to the variation of some parameters such as launch frequency, percentage of compliance with regulations, and implementation of active removal missions. However, White and Lewis [4] showed that the effect of remediation measures is not the same for the population of objects larger than 10 cm compared to the population between 5 and 10 cm. The latter may still increase even when the former is expected to decrease. In other words, focusing only on the large fragments may lead to an underestimation of the collision risk. In fact, also *small* fragments can pose a relevant hazard to spacecraft. In particular, objects larger than 1 mm are yet able to interfere with operational spacecraft causing anomalies and objects larger than 1 cm can even destroy a satellite in case of collision [5]. Recently, McKnight et al. [6] highlighted how the so-called *lethal non-trackable* objects may become the leading factor in the decrease of flight safety.

When aiming to get a global picture of space debris down to 1 mm, models currently employed to study the debris evolution cannot be simply *extended* to consider also small fragments. In fact,

the number of objects larger than 1 cm in LEO is around 500 000 and more than one hundred million objects larger than 1 mm are thought to be in orbit around the Earth [3]. These numbers are too large to consider a piece-by-piece analysis of the debris population feasible as the resulting computational time would be prohibitive. For this reason, some existing models, such as Rossi et al. [7], sample the small fragments and define some representative objects, which are the only ones to be propagated. Then, the representative objects need to be re-converted into a distribution of small fragments or in a value of fragment density to compute the resulting collision probability.

This work discusses the applicability of a novel alternative method, where the small fragments are modeled in terms of their spatial density. This approach presents two main advantages. Firstly, the proposed method, CiELO (debris Cloud Evolution in Low Earth Orbits), operates directly on the spatial density, which can be used to compute the contribution to the collision probability due to small fragments. Secondly, the formulation in terms of spatial density admits an analytical solution for the evolution of the fragment density in the Low Earth Orbit (LEO) region where the effect of drag is dominant.

The method will be briefly outlined in Section II, while Section III-IV present the most recent improvements in the proposed approach. Finally, Section V discusses some possible applications of the method, such as the study of the consequences of some real breakups on a set of targets and the analysis of the worst conditions for a fragmentation considering the resulting collision probability for the target set.

II. Method overview

An analytical approach to the study of space debris population in LEO was proposed by McInnes [8]. His approach is based on the application of the continuity equation to obtain an explicit expression for the global debris spatial density in time. In this work, instead, this approach is used to model a single fragmentation event and assess its consequences in terms of the resulting fragment spatial density and the change in the collision probability for other spacecraft.

For this purpose, McInnes' analytical propagation [8] is included as one of the building blocks (Fig. 1) required to model a fragmentation event from its beginning (the breakup) to the long term

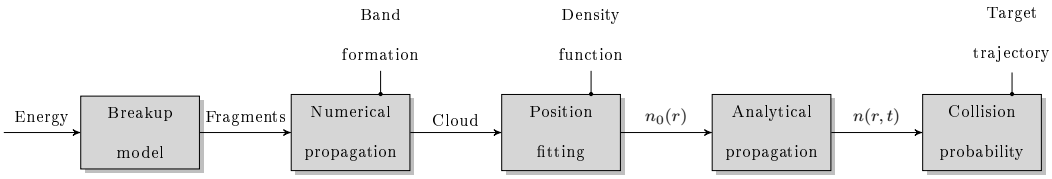

Fig. 1 CIELO building blocks.

evolution. The proposed method is here briefly summarized through a short description of the first four blocks in Fig. 1; further details on the overall method can be found in [9]. The rest of the paper will focus on the fifth block regarding the computation of the collision probability.

The simulation of a fragmentation starts with the generation of the fragments through the application of the NASA breakup model [10, 11], considering only fragments with size between 1 mm and 10 cm. Once the fragments are generated, their orbital parameters are numerically propagated to model the initial phase of the cloud evolution when the Earth's oblateness is the dominant driver [12, 13]. The numerical propagator used in this phase is PLANODYN [14], a semi-analytical propagator based on the averaged variation of the orbital elements in Keplerian elements. In particular, for this work, only the following perturbations are considered: the secular effect of the Earth's oblateness [15], considering the J_2 term only, and the effect of the atmospheric drag, considering the average variation of the parameters along one orbit as obtained by King-Hele [16].

The numerical propagation is stopped once the fragments are spread over 360 degrees and form a band around the Earth. The time required for this transition can be estimated through Ashenberg's theory [17]. From this moment, the problem can be studied with the analytical method proposed by McInnes [8], changing the point of view from the single fragments to the whole cloud. This requires the information on the position of all the fragments to be converted into a continuous density function $n_0(r)$. A detailed discussion on the functions used for this purpose is provided in Section III.

The long term evolution of the cloud is obtained by applying the continuity equation to model the effect of atmospheric drag [8]. Using n to indicate the fragment spatial density, the continuity

equation is written as

$$\frac{\partial n(r,t)}{\partial t} + \nabla \bullet \mathbf{f} = 0, \tag{1}$$

where $\mathbf{f} = n\mathbf{v}$ is the vector field that models drag and $\nabla \bullet \mathbf{f}$ is its divergence.

Assuming that the system can be considered spherically symmetrical, it can be studied through only one coordinate, the geocentric radius r. Therefore, $\mathbf{f}$ has only one component, $f_r = v_r n(r,t)$, with v_r is the radial velocity due to drag. Introducing the hypothesis of circular orbits for the fragments and considering an exponential model for the atmosphere, an explicit expression for the fragment spatial density is found

$$n(r,t) = n_0(r_i)\frac{r_i^2 v_r(r_i)}{r^2 v_r(r)} \tag{2}$$

where r_i is the function

$$r_i = g(r,t) = H \log G(r,t) + R_H \tag{3}$$

that is derived from inverting the expression of the characteristics $G(r,t)$ at the *initial* time $t = 0$. Further information on the mathematical details can be found in [9]. Through Eq. 2, the value of the density at a certain altitude and at a certain time instant is immediately known and it can be used to compute the collision probability for a spacecraft crossing the cloud as explained in Section IV.

It should be observed that the hypothesis of circular orbits for the fragments limits the applicability of the method. Firstly, it can be applied only to model fragmentations starting from circular orbits, where the majority of the fragments have an eccentricity lower than 0.05 both in the case of explosions and of collision. Circular orbits are, in any case, where the vast majority of cataloged objects can be found [2] and where historically most of the fragmentations have started [18]. In addition, the hypothesis of circular orbits limits the altitudes where the method is applicable because at low altitude ($< 800\,\text{km}$) eccentricity has a large influence on the accuracy of the propagation [9]. An extension of the method able to deal also with the distribution in eccentricity is currently under development [19]. Despite this constraint, the analytical method can be still applied to study the regions in LEO with the highest debris density, which are around and above 800 km [2]. At these altitudes also the effect of solar radiation pressure should be considered as this force can reach the

same order of magnitude as drag for objects with large area-to-mass ratio. Future work will aim to include also the effect of this perturbation in the analytical propagation, whereas the current work considers the effect of atmospheric drag only and intend to validate the use of the spatial density approach to compute the collision probability.

III. Density definition

A. Fragment spatial density

The simplest approach to define the initial condition for the analytical propagation would be to set it equal to the actual distribution of fragments with altitude at the time of the band formation (T_B). However, in this way, the initial condition would depend on the moment when the band is considered formed and on the specific run of the breakup model used to simulate the fragmentation. In fact, the NASA breakup model contains some random parameters to describe the distribution of the fragments. A Monte Carlo approach could be adopted to give statistical meaning to the results.

An alternative approach is adopted here. The positions of the fragments is not set directly as initial condition, but the information on the fragments' orbital parameters (namely, the semi-major axis a, the eccentricity e, the inclination i) is used to describe the fragment distribution in space, whereas the other parameters (i.e., the longitude of the ascending node Ω, the argument of the periapsis ω and the mean anomaly M) are randomized within the cloud. In this way, the dependence on the band formation time and on the run of the breakup model is reduced.

The conversion from the orbital parameters to the spatial density can be done by using the expressions by Kessler [20] and Sykes [21], both derived from the work of Öpik [22]. They express the probability of finding a particle, at a certain distance from the central body r and a certain latitude β, knowing its orbital parameters a, e, i, and assuming that the other parameters can be considered randomly distributed. Note that when a cloud generated by a breakup is simulated, the energy will spread differently among the fragments, so the mean anomaly M is the one randomly distributed. These expressions depend only on geometry, so they have been applied to different problems related to space debris [23, 24], the design of disposal trajectories [25], but also asteroids [21] and Jupiter's outer moons [20]. Moreover, the dependence on the distance and on the latitude

can be described separately, which is particularly useful in the current application as the evolution of the two parameters occurs with different time scales and drivers.

According to Kessler's [20] and Sykes' [21] expressions, the spatial density in a particle band can be expressed as

$$S(r, \beta) = s(r) f(\beta) \tag{4}$$

where

$$s(r) = \frac{1}{4\pi r a^2} \frac{1}{\sqrt{e^2 - \left(\frac{r}{a} - 1\right)^2}} \tag{5}$$

$$f(\beta) = \frac{2}{\pi} \frac{1}{\sqrt{\cos^2 \beta - \cos^2 i}}, \tag{6}$$

so, if only the dependence on the distance is considered, Eq. 5 can be used to build the initial condition $n_0(r) = s(r)$. In this section only the expression as a function of the distance r is analyzed, whereas the role of latitude is discussed in Section III C. Appendix A explains how to derive the expression of the spatial density as a function of the orbital elements (Eq. 5) starting from a set of fragments equally distributed in mean anomaly.

When modeling the cloud produced by a breakup, the dispersion of the orbital parameters a, e among the fragments should be considered. This means that Eq. 5 cannot be applied directly to describe the cloud density using the initial value of a, e of the orbit where the fragmentation occurred. Instead, it should be applied to each fragment to take into account how the energy is distributed among them; the total density is then obtained by simply summing the contribution of each fragment

$$n(r) = \sum_{j=1}^{N_f} n_j(r).$$

B. Validation of the density expression

The expression for the density was initially tested considering its accuracy in modeling the initial density profile, which is the distribution of the fragments at the band formation. This was done both on single runs of the NASA breakup model and on an average distribution obtained with ten runs of the breakup model.

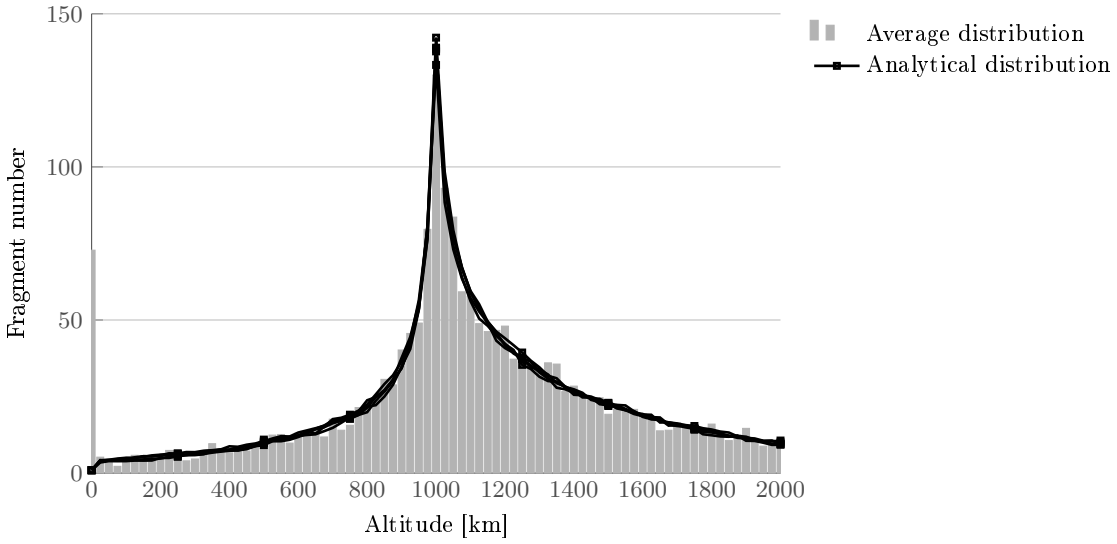

Fig. 2 Average fragment spatial distribution at the band formation over ten runs of the breakup model and distribution obtained from Eq. 5. Altitude bin size equal to 25 km.

Fig. 2 shows the test performed on ten different runs of the NASA breakup model for a non-catastrophic collision with energy equal to 100 kJ, occurring on a circular equatorial orbit at 800 km. The grey bars represent the average distribution of fragments from the numerical propagation and the black lines the resulting profiles applying Eq. 5.

The comparison is expressed in terms the number of fragments in an altitude shell of width equal to 25 km, so the result of Eq. 5 is multiplied by the volume of the spherical shell $V_{\text{shell}} = \frac{4}{3}\pi(r_+^3 - r_-^3)$ where $r_\pm = r \pm \Delta r$ with r center of the altitude bin and Δr bin width. From Fig. 2 it is possible to observe how Eq. 5 captures the general shape of the distribution and shows low variability among the different runs. This observation is important because it confirms that the results obtained with the proposed analytical method have a limited dependence on the specific run of the breakup model used to model a fragmentation.

This aspect was studied more in detail evaluating also the variability of the results after the propagation at different altitudes. For the validation, ten runs of the breakup model are used to simulate a fragmentation; the resulting debris cloud is followed up to 1000 days after the band formation, when the difference with the numerical propagation is measured. The reference case is set as the density profile obtained by averaging the result of the numerical propagation over the ten

runs of the breakup model. The results of the analytical propagation are compared to this reference case but they are built starting from the output of a single run of the breakup model, so that the variability of the results can be evaluated.

PlanODyn [14] is used as numerical propagator also in this case, with the same settings described in Section II. In particular, the effect of solar radiation pressure is not included in the numerical propagation, even if its effect is important at altitudes larger than 800 km. Future work will aim to validate the analytical propagation considering also this perturbation and will try to include its effect in the continuity equation.

For both the propagation methods, numerical and analytical, the predicted number of fragments still in orbit is computed and the relative error on this estimation $\mathrm{err_t}$ is used as a measure of the accuracy of the analytical method. In detail, $\mathrm{err_t}$ is computed as

$$\mathrm{err_t} = \frac{|\int n_A(r)\,\mathrm{d}r - \int n_N(r)\,\mathrm{d}r|}{\int n_N(r)\,\mathrm{d}r}$$

where $n_N(r)$ is the profile of the spatial density obtained with the numerical propagation and $n_A(r)$ is the one from the analytical propagation. Another indicator used to measure the accuracy is the relative error $\mathrm{err_p}$ on the height of the peak in the distribution of fragments with altitude,

$$\mathrm{err_p} = \frac{|\max n_A(r) - \max n_N(r)|}{\max n_N(r)}.$$

The values of $\mathrm{err_t}$ and $\mathrm{err_p}$ for fragmentations at different altitudes are shown in Fig. 3, where the error bars indicate the maximum and the minimum error among the ten density profiles obtained with the analytical propagation.

From the curve for $\mathrm{err_t}$ it is possible to observe that the variability with the run of the breakup model is very limited. For $\mathrm{err_p}$ the variability is larger, but the error is in general lower than $\mathrm{err_p}$. This shows that the proposed analytical model gives a reliable representation of the cloud evolution without requiring multiple runs of the breakup model. This represents an advantage with respect to other debris propagation methods that relies on multiple Monte Carlo runs.

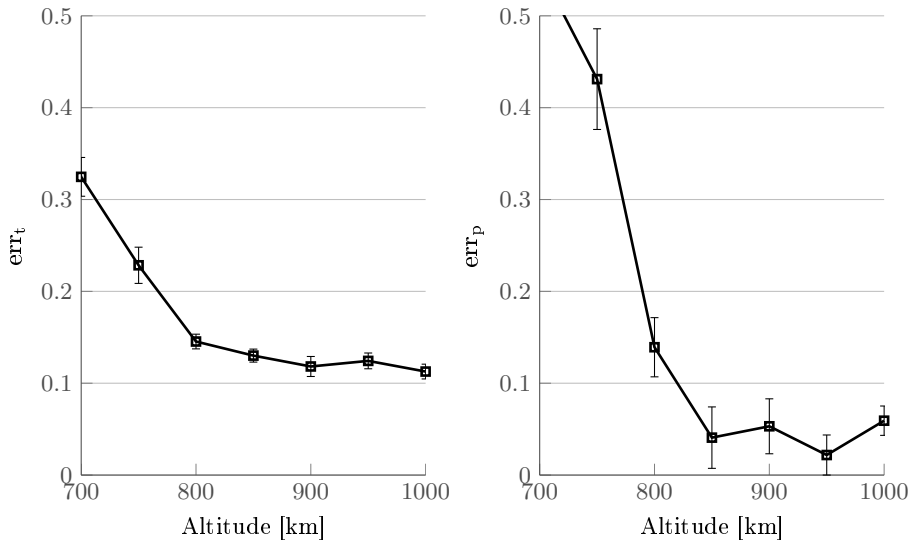

Fig. 3 Relative error on the total fragment number ($\mathbf{err_t}$) and on the density peak ($\mathbf{err_p}$) of the analytical model at different altitudes.

C. The dependence on latitude

As stated in Section III, the correct representation of the cloud spatial density requires considering also the distribution in latitude. However, in this work a constant distribution in latitude is assumed, similar to what is already done by Kessler [24]. This approximation is chosen because the purpose of this method is to study the long term (i.e., years) effect of a fragmentation, whereas the latitude of a target spacecraft crossing the cloud evolves in a much shorter time scale (i.e., hours). Following correctly the target latitude would require very short time step for the integration, eliminating or reducing the advantage of having a fast propagator for the fragment cloud.

However, it is important to remark that the analytical method is able to deal also with the distribution in latitude. In fact, applying the general solution for a 2D formulation of a continuity equation problem to the current application, the expression for the density can be written as

$$\tilde{n}(r,\beta,t) = \tilde{n}_0(r_i,\beta_i)\frac{v_r(r_i,\beta_i)v_\beta(r_i,\beta_i)}{v_r(r,\beta)v_\beta(r,\beta)} \tag{7}$$

where $\tilde{n}_0$ is the initial distribution, r_i, β_i are functions obtained by inverting the characteristic lines at initial time $t = 0$, v_r, v_β are respectively the expression of dr/dt and $d\beta/dt$ due to the effect modeled by the continuity equation, i.e., drag. Therefore, in this case, where the effect of drag on

quasi-circular orbits is considered,

$$\frac{dr}{dt} = -\varepsilon\sqrt{R_H}\exp\left(\frac{r-R_H}{H}\right) \tag{8}$$

$$\frac{d\beta}{dt} = 0 \tag{9}$$

meaning that v_r depends only on r and the distribution in latitude is not directly affected by drag. As a result, Eq. 7 can be written as

$$\tilde{n} = \tilde{n}_0(r_i,\beta)\frac{v_r(r_i)}{v_r(r)}. \tag{10}$$

The expression for $\tilde{n}_0(r_i,\beta_i)$ is simply the one given by Kessler [20] and Sykes [21], so using the expressions in Section III,

$$\tilde{n}_0(r_i,\beta_i) = S(r_i,\beta) = s(r_i)f(\beta) \tag{11}$$

and finally

$$\tilde{n}(r,\beta,t) = f(\beta)\frac{s(r_i)v_r(r_i)}{v_r(r)}. \tag{12}$$

Similarly to what is done for $s(r)$, $f(\beta)$ can be built from the distribution of the fragments at the time of band formation.

In this work, as explained before, the choice was not to follow in detail the evolution of the target latitude: the collision probability is computed using an average value of the fragment density, which depends only on the radial distance and not on the latitude.

The average density value can be found computing once the integral average of $f(\beta)$ over one orbit period and apply it to rescale the spatial density at any time, applying again the hypothesis that the fragments' and the target's inclinations are not changing. The dependence of the latitude β on the orbital parameters is expressed by

$$\beta = \arcsin\left(\sin\left(\omega+\nu\right)\sin i\right) \tag{13}$$

where ω, ν, i refer to the argument of perigee, the true anomaly and the inclination of the target spacecraft crossing the cloud. Introducing the argument of latitude $u = \omega + \nu$ and writing the expression for the case of circular orbit, the scaling factor of the spatial density can be computed as

$$\bar{f} = \frac{1}{2\beta_{\max}}\int_0^{2\pi}\frac{\mathrm{d}u}{\sqrt{\cos^2\left(\beta(u)\right)-\cos^2\left(\beta_{\max}\right)}} \tag{14}$$

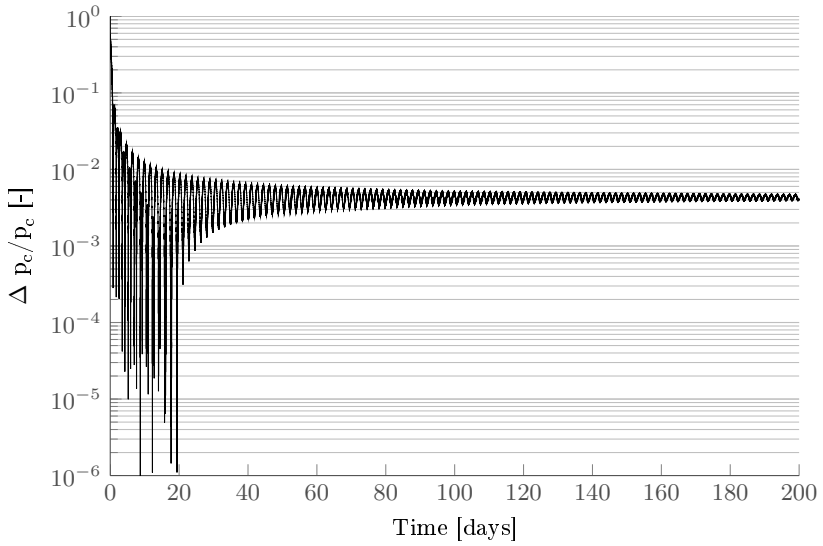

Fig. 4 Relative error on the collision probability due to the averaging in latitude.

where $\beta(u)$ is given by Eq. 13. $\beta_{\max}$ is the maximum latitude covered by the band. For non-equatorial orbits $\beta_{\max}$ is put equal to the inclination where the fragmentation occurred i_F if $i_F \leq \pi/2$ and equal to $\pi - i_f$ otherwise. This follows from the band characterization proposed by McKnight [12] and the observation that, with the current hypotheses (e.g., non-rotating atmosphere), the fragment inclination is not affected by drag and so it is constant. For equatorial orbits, $\beta_{\max}$ is put equal to the maximum inclination reached by the fragments because of the breakup.*

This approach was tested by performing a simulation where the spatial density and the collision probability ($p_{c,f(\beta)}$) are computed considering the dependence on the latitude and using a very short time step, equal to five minutes.† In this way, for each target orbit there are at least 20 integration points and the value of β can be considered representative of the time-step. This result is compared to the simulation ran with a time step equal to one day, where only the dependence on the geocentric distance is considered and the scaling factor from Eq. 14 is applied. The collision probability obtained in this way is indicated with $p_{c,\bar{f}}$.

---

* This can be done for any inclination of the parent orbit and this approach was compared with the results obtained setting the maximum covered latitude equal to the parent orbit inclination. The latter gives actually a distribution closer to the observed one and is, therefore, implemented.

† Observe that using this large number of points results in a remarkable increase in the RAM required to run the simulation in a such a way that high-performance computing was employed for this validation. If the analytical method is instead used on a normal machine, then a reasonable time-step needs to be chosen.

The result of the comparison is presented in Fig. 4: it shows the relative error

$$\frac{\Delta p_c}{p_c} = \frac{|p_{c,\bar{f}} - p_{c,f(\beta)}|}{p_{c,f(\beta)}} \tag{15}$$

introduced by Eq. 14 on the collision probability. The simulation refers to a target with inclination equal to $i_T = 60$ degrees crossing a cloud generated from an orbit with equal inclination ($i_F = 60$ degrees).

It is possible to observe how the difference between the two methods is limited, with the relative error that oscillates around a value equal to 0.004. Therefore, Eq. 14 is an effective way to model the long term evolution of the collision probability without following the target latitude. For this reason, this approach will be used in the following results where the spatial density is always computed as

$$S(r) = \bar{f}s(r).$$

IV. Collision probability computation

Once the cloud density at any time is known, it is possible to evaluate its effect on the collision probability for a spacecraft that crosses the cloud. The computation of the collision probability is based on the average number of collisions N in an interval of time [20]. This number is then used to obtain the cumulative collision probability for the target spacecraft through a Poisson distribution

$$p_c(t) = 1 - \exp(-N) \tag{16}$$

following the common analogy with the kinetic gas theory [12, 23]. According to this analogy, the collisions between a target and a distribution of objects, in this case the fragments in a cloud produced by a fragmentation event, can be modeled similarly to the collisions among molecules within an inert gas [26]. This requires that the probabilities of events at different times are independent (fragment random motion) and that the probability of collision during a certain time interval is proportional to the length of the time interval (large number of fragments). This approach has been criticized for example by Chan [27], who observes how the spatial density of the fragments and the mean free path of the target have a very different ratio in the case of gases and in the one of space debris. Jenkin [26] also criticizes this approach if used in the first phases of the cloud evolution, when the fragments' trajectories are highly correlated. In our application, the analogy is applied at

a later stage of the cloud evolution, when the motion of the fragments has already been randomized. Moreover, other approaches to the computation of collision probability, such as the one proposed by Chan [27], should be feasible if they are based on a dependence of the number of collisions on the fragment spatial density.

In the traditional approach, the average number of collisions N in a given interval of time $\Delta t = t - t_0$ can be written as

$$N = F\sigma\Delta t \tag{17}$$

where F is the flux of particles and σ represents the collisional cross-sectional area [20]. This last parameter is usually defined considering the dimensions of both the colliding objects [20], but here only the target spacecraft area A_T is considered because the fragments are much smaller than it, so $\sigma \approx A_T$.

The flux F is equal to

$$F = n(r,t)v \tag{18}$$

where $n(r,t)$ is the value of the spatial density obtained with the CiELO method explained in Section II and applying the scaling factor due to the distribution in latitude. v is the average relative velocity between the targets and the fragments.

To keep the formulation simple and dependent only on the radial distance, a set of hypotheses is introduced to obtain the expression of v.If a single fragment is considered, v can be obtained from the rule of cosines

$$v^2 = v_T^2 + v_F^2 - 2v_T v_F \cos\phi \tag{19}$$

where v_T and v_F are respectively the orbital velocities of the target and of the fragment with respect to the central body; ϕ is the angle between the two vectors $\mathbf{v_T}$ and $\mathbf{v_F}$. v_T is known from the propagation of the target trajectory; v_F is a piece of information that is lost with the analytical propagation. However, the propagation of the fragment cloud is done under the hypothesis of quasi-circular orbits, so

$$v_F \approx v_{\text{circ}} = \sqrt{\frac{\mu}{r}}. \tag{20}$$

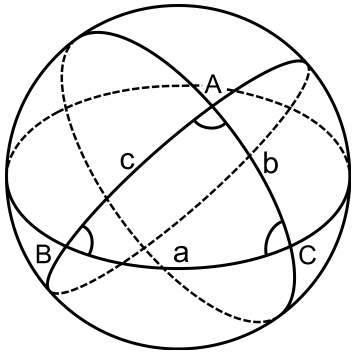

Fig. 5 Generic spherical triangle.

The angle ϕ can be related to the geometry of the two orbits too. In fact, the intersection between two circular orbits with the same radius can be represented by the spherical triangle in Fig. 5 where B is the ascending node of the target orbit and C the ascending node of the fragment orbit. Therefore,

$$B = i_T \quad C = \pi - i_F;$$

also $a = \Delta\Omega$, so the spherical triangle can be solved with the law of cosines to find the angle A

$$\cos A = \sin B \sin C \cos a - \cos B \cos C \tag{21}$$

$$= \sin(i_T) \sin(i_F) \cos(\Delta\Omega) + \cos(i_T) \cos(i_F) \tag{22}$$

Eq. 22 can be used to provide a unique value of ϕ for a given configuration of target and fragments in terms of their inclinations. In fact, given that Ω is uniformly distributed among the fragments, the average relative velocity $\Delta\bar{v}$, can be found computing the integral mean of the function

$$\Delta v = \sqrt{v_T^2 + v_F^2 - 2 v_T v_F \left[\sin(i_T) \sin(i_F) \cos(\Delta\Omega) + \cos(i_T) \cos(i_F)\right]} \tag{23}$$

for $\Delta\Omega$ from 0 to 2π. By putting

$$\chi = v_T^2 + v_F^2 - 2 v_T v_F \cos(i_T) \cos(i_F) \qquad \eta = 2 v_T v_F \sin(i_T) \sin(i_F)$$

the average value of the relative speed can be written as

$$\Delta\bar{v} = \frac{2}{\pi} \sqrt{\chi + \eta}\, \mathrm{E}\left[\frac{2\eta}{\chi + \eta}\right], \tag{24}$$

where $\mathrm{E}[x]$ is the complete elliptic integral of the second kind.

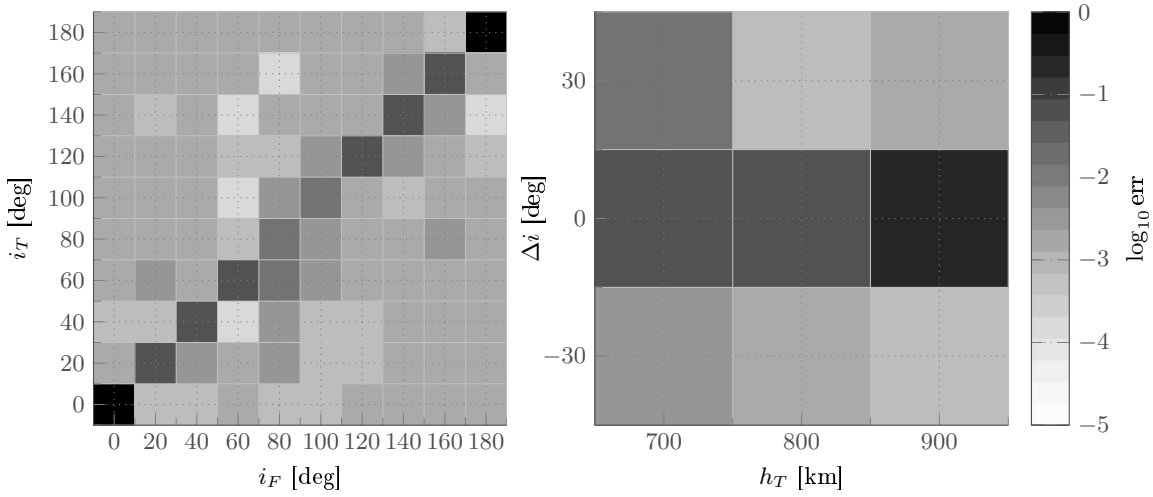

Fig. 6 Relative error in the estimation of the relative velocity between target and fragments for several configurations.

The approximation for Δv was validated for different geometries of the target and fragment orbits. The results of the validation are shown in Fig. 6, where the metric used to measure the method accuracy is

$$\overline{\text{err}}_{\text{rel}} = \frac{\int |\Delta v_A - \Delta v_N| \, \mathrm{d}t}{\int \Delta v_N \, \mathrm{d}t}, \tag{25}$$

where Δv_N is the estimation of the velocity obtained using a numerical procedure that computes the distance and the relative velocity between the target and each fragment; Δv_A is the analytical estimation obtained from Eq. 24. Basically, Eq. 25 measures if the analytical approximation is able to capture the average value of the relative velocity, which is considered to be the most relevant parameter in a long-term study of the collision probability.

The plot on the left in Fig. 6 refers to different combinations of inclinations for the target (i_T) and the fragments (i_F), while their initial altitude is the same and equal to 800 km. As one could expect, Eq. 24 does not work for equatorial orbits, where $\Delta\Omega$ is not defined; for those cases $\overline{\text{err}}_{\text{rel}} \approx 0.3$ whereas it is lower than 0.08 for all the other cases. The estimation of Δv in the cases with equatorial orbits could be improved if information on the distribution of the fragments in eccentricity were available. The extension of the method towards this direction is in progress, so future work aims to fully develop the method to consider the effect of eccentricity.

The plot on the right in Fig. 6 shows instead the results for different choices of the orbit

inclinations, with $\Delta i = i_F - i_T$, and of the target altitude, with the fragmentation starting again at 800 km. Also in this case the error is generally low, but it tends to increase with the altitude difference for orbits with the same inclination. In addition, it was verified that $\overline{\mathrm{err}}_{\mathrm{rel}}$ is lower than 10% for the cases discussed in Section V.

Here we would like to highlight that the expression in Eq. 24, even with its limits in terms of applicability, appears as an important improvement of the method compared to its previous formulation [28], where it was assumed that the impact angle between the target and the fragments is always equal to 90 degrees. This hypothesis was conservative and it largely overestimated the relative velocity Δv, whereas the expression in Eq. 24 provides a more realistic estimation of Δv.

V. Collision scenarios

Thanks to its limited computational time and its good accuracy, the proposed method CiELO can be applied to study the collision probability due to small fragments in many different scenarios. The use of CiELO is proposed for following three applications. First, it can study the effect of a breakup on different target spacecraft. Second, it can be used to build, for each target spacecraft or for a whole set of targets, a *map* of collision probability by varying the inclination and the altitude of the simulated breakup. Third, the analytical method can be applied to generate a *matrix of influence* among a selected set of targets.

The targets used for the simulations are listed in Tab. 1: they were extracted from a list prepared by IFAC-CNR, ISTI-CNR and University of Southampton for a study sponsored by the European Space Agency [29]. The objects in Tab. 1 are the ten spacecraft with the largest collision probability and they are sorted by their semi-major axis. Note that the list of target spacecraft can be selected depending on the desired application.

A. Single event simulation

The first application of the method is the evaluation of the consequences of a breakup on the target list in Tab. 1, considering the collision probability associated with fragments larger than 1 mm.

For this application, two recent small breakups are considered [30], whose parameters are re-

Table 1 List of target spacecraft [29] for the collision probability analysis.

ID Target	h_p [km]	h_a [km]	i [deg]	Mass [kg]	Size [m]
1	816.0959	818.9741	98.73	4090	6.91
2	818.5311	832.9389	98.83	2490	5.17
3	804.0385	858.8315	98.83	1000	4.46
4	822.4681	865.8019	70.90	3220	4.49
5	946.4051	986.0649	82.91	1420	4.06
6	934.9528	998.1172	82.95	1420	4.06
7	964.0951	990.5749	82.95	1420	4.06
8	960.1156	1005.754	82.93	1420	4.06
9	968.9735	999.8965	82.94	1420	4.06
10	1099.8350	1099.8350	63.00	1000	2.41

ported in Tab. 2. The value in the last column is an estimation of the parameter M used in the NASA breakup model as a measure of the energy of the breakup [10]. For non-catastrophic collisions it is defined as the product between the mass of the smaller object m_p and the square of the collision velocity v_{coll} [11]

$$M_E[\text{kg}] = m_p[\text{kg}]v_{\text{coll}}^2[\text{km/s}]/1[\text{km/s}].$$

From this parameter the fragment size distribution for a collision can be described through the expression

$$N(L_c) = 0.1(M_E)^{0.75}L_c^{-1.71} \tag{26}$$

where L_c is the fragment characteristic length and $N(L_c)$ is the number of fragments of size equal or larger than L_c. The parameter M is here estimated considering that for the two breakups the number of fragments added to the debris population catalog is known (respectively 35 objects for Cosmos 1867 and 9 objects for Cosmos 2428)[‡]. Therefore, assuming that the tracked fragments are larger than 5 cm, the value of M is obtained inverting Eq. 26 and then the number of fragments N_F

[‡] Values updated from `https://www.space-track.org/`

in the desired size range (1 mm-10 cm) is obtained applying again Eq. 26 with the computed value of M. Observe that the total number of fragments shown in Tab. 2 is very high and there is not a general consensus on the reliability of the NASA breakup model in the studied size range. Some modifications of the model are available in literature [31], but the original NASA model is used because the purpose of this work was not to develop a new breakup model, but rather to show the possible applications and the advantages of using a formulation based only on the spatial density. The implementation of the NASA model used in this work was validated with the comparison to the available data on other implementations [32].

Table 2 Parameters of two recent small breakups [30].

Spacecraft	h_p [km]	h_a [km]	i_0 [deg]	$N_{L_c>5\,\mathrm{cm}}$	M [kg]	N_F
COSMOS 1867	775	800	65	35	2.665	28138
COSMOS 2428	845	860	71	9	0.436	7235

The effect of the breakups on the target in the list is shown in Fig. 7, which shows the cumulative collision probability caused by fragments larger than 1 mm from the time of band formation up to five years afterwards. The study of a single case in Fig. 7 for the COSMOS 1867 event was obtained with an average computational time of 9.45 minutes on a cluster with 4 processors; the average computational time is instead equal to 7 minutes for the COSMOS 2428 cases. Most of the propagation time is required for the propagation of the fragments from the breakup to the band, so the computational effort is required only once to generate the fragment cloud, which can be saved and superimposed on each target spacecraft trajectory.

For the first breakup (COSMOS 1867), the resulting collision probability p_c is shown in Fig. 7(a): it is possible to observe that the first four spacecraft are the most affected by the fragmentation. This is explained by two factors: firstly, SC1 and SC2 have the largest cross-sectional area, and secondly the first four spacecraft are both at the lowest altitudes and the shortest radial distance from the fragmentation location. In particular, it is possible to observe an exponential relationship between the spacecraft altitudes and the final values of the collision probability after five years.

A similar behavior can be observed also for the second breakup (COSMOS 2428) in Fig. 7(b),

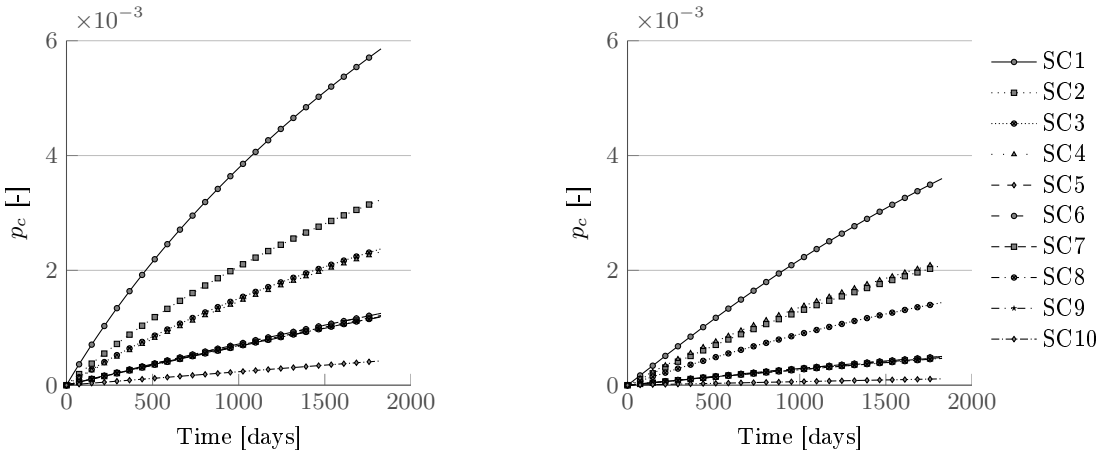

(a) COSMOS 1867

(b) COSMOS 2428

Fig. 7 Resulting collision probability from the two breakups on the targets in Tab. 1 including fragments down to 1 mm**.**

which shows the effect of inclination. In fact, the inclination of COSMOS 2428 is very similar to the one of SC4, which, in this case, has a slightly higher collision probability than SC2 even if the latter has a larger cross-sectional area.

B. Maps of collision probability

The collision risk for a spacecraft can be studied also from a different point of view: instead of focusing on a single breakup, here the location of the breakup is changed to highlight the effect of the breakup conditions on the collision probability. In particular, here the altitude and the inclination of the fragmentation are changed and this allows defining the most dangerous regions for a collision to occur for all the targets in Tab. 1. Other parameters (e.g., time, fragmentation energy) may be considered with the same approach.

Fig. 8 shows, for example, the study done for the spacecraft SC4 for fragmentations of 100 kJ, including all the fragments down to 1 mm. The peak in the collision probability is slightly above the altitude of the spacecraft semi-major axis ($a_{\mathrm{SC4}} = R_E$+844 km) and for inclinations i_F such that $\sin(i_F) = \sin(i_{\mathrm{SC4}})$. Under this condition, the spacecraft will spend a part of its orbit at latitudes where the cloud density is maximum. The collision probability is high also for inclinations where $\sin(i_F) > \sin(i_{\mathrm{SC4}})$ because in these cases the spacecraft is always inside the band formed by the

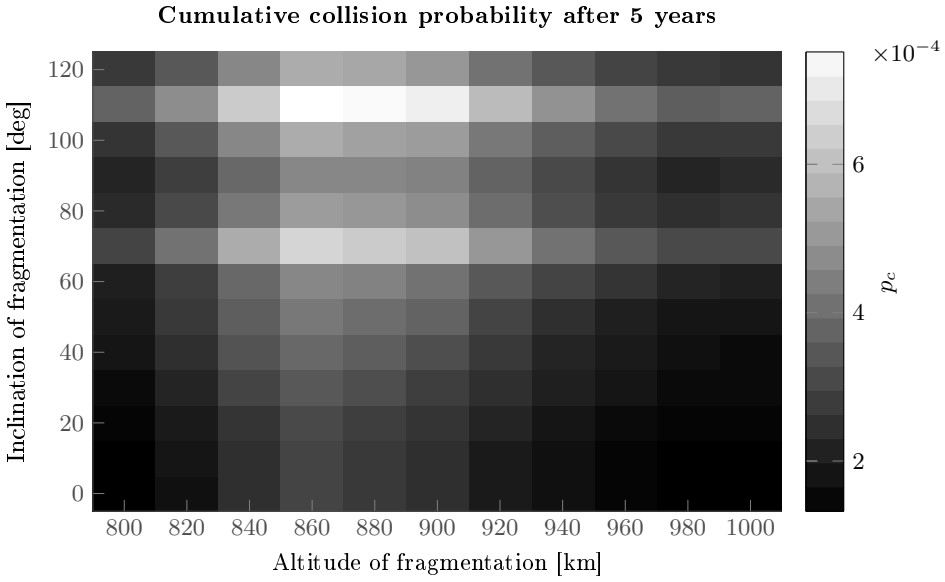

Fig. 8 Collision probability map for SC4 for fragmentations of 100 kJ, including all the fragments down to 1 mm.

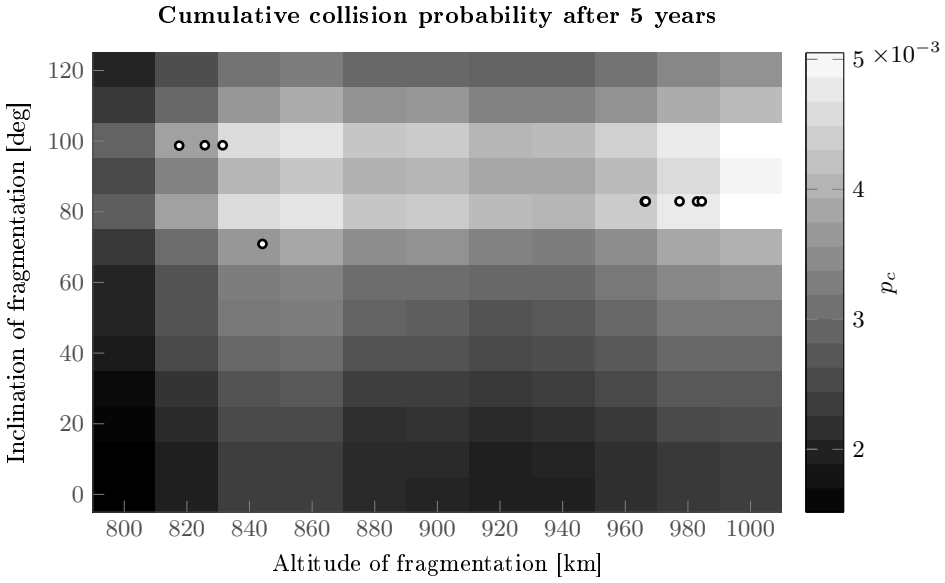

Fig. 9 Total collision probability map for the targets in Tab. 1 for fragmentations of 100 kJ, including all the fragments down to 1 mm. The markers indicate the targets.

fragments. As expected, fragmentations at higher altitudes than SC4 have a larger effect than the ones at lower altitudes. In fact, over time drag tends to reduce the fragments altitude and the fragments initially at altitudes higher than SC4 decay towards the target orbit.

The same analysis was performed for all the targets in Tab. 1 to obtain the map in Fig. 9,

where the markers indicate the targets. Here it is possible to observe two peaks in the collision probability, corresponding to the two bands in altitude where the targets are grouped: the first from 817 to 844 km for SC1-4, the second from 966 to 984 km for SC5-9. Observing the first peak in altitude ($h \approx 840$ km), it is possible to notice that the distribution of collision probability is not symmetrical around the peak: in fact, fragmentations at higher altitudes (e.g., 880 km) have a larger effect than the ones at lower altitudes (e.g., 800 km) as already discussed for Fig. 8. It is also possible to observe that the collision probability is still relatively high around $h = 820$ km, mainly because of the presence of SC1, whose large cross-sectional area has a large influence on the total collision probability.

As observed in Fig. 7(b) and Fig. 8, the fragmentations with $\sin(i_F) = \sin(i_T)$ have a large effect on the total collision probability because of the distribution of objects with latitude. Eight out of ten spacecraft in Tab. 1 have $\sin(i_T) \approx \sin(82°) = \sin(98°)$, so at these inclinations two clear bands of high collision probability are present. Compared to previous results obtained with the continuity equation approach [33], the bands are more evident because the expression in Eq. 14 takes into account the different time of residence of the target inside regions with high spatial density when its inclination is similar to the one of the fragmentation. Similar to Fig. 8, the collision probability is high also in the whole inclination band between 80 and 100 degrees, which corresponds to fragmentations for which all the targets are always inside the fragment band.

A map such as the one in Fig. 8 is obtained with a computational time of 3.66 hours in average[§] on a cluster with 4 processors. The process can be easily automatized and parallelized to study a list of targets and obtain a global map as the one in Fig. 9. These maps may be useful to study both operational and non-operational targets to understand under which conditions a fragmentation has the largest effect on the spacecraft. Moreover, the global maps can highlight the most critical areas in terms of influence on the whole spacecraft population and can be used, for example, to identify interesting candidates for active debris removal. Note that the targets to build the global map can increased or some representative objects of the whole population can be chosen.

[§] among the ten cases

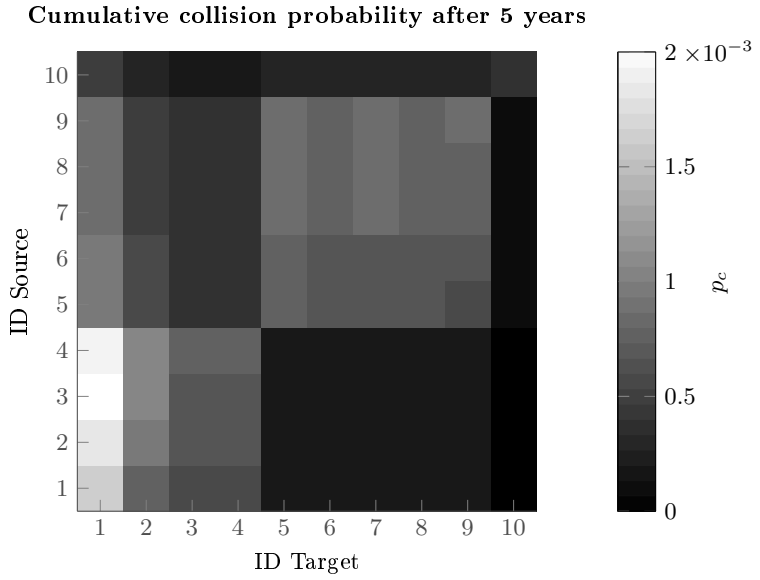

Fig. 10 Influence matrix showing the cumulative collision probability for ten studied spacecraft.

C. Influence matrix

The *influence matrix* is proposed to study the following situation: a small breakup caused by a non-catastrophic collision with one of the spacecraft in Tab. 1, generates a fragment cloud that can interfere with other spacecraft. Each spacecraft in Tab. 1 is treated as a potential target and its collision probability due to the fragment cloud is computed after a certain time. This process is repeated scrolling through the whole list of spacecraft in Tab. 1 to obtain a picture of how each spacecraft affects the collision probability of the other ones.

Fig. 10 shows the resulting influence matrix for the spacecraft in Tab. 1 considering a fragmentation of 100 kJ and plotting the resulting collision probability after five years. Here it is important to specify that, as the proposed method is able to provide an analytical expression for the density only after the band is formed, the collision probability is computed starting from that moment. This means that the collision probability may be underestimated for satellites such as SC5-SC9 that have very similar orbits and that may start to interact before the band is formed.

The sum of the collision probabilities, over all the targets, due to the same source can be used as an index of the spacecraft *influence*; similarly, the sum of the collision probabilities for one target from all the sources can be used as an index of its *vulnerability*. In formulas, $I(i, j)$ is the element

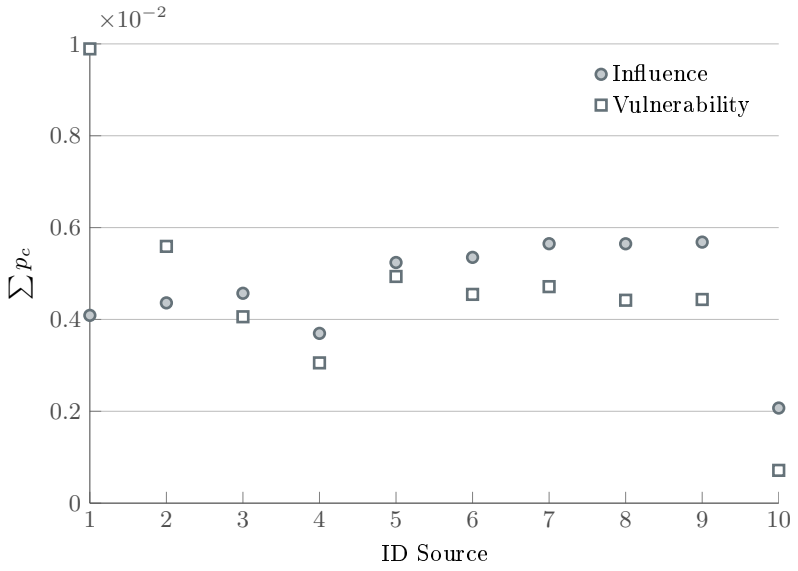

Fig. 11 Sum of the generated collision probability for the scenarios in Fig. 10.

of the influence matrix that expresses the cumulative collision probability of the object j due to a fragmentation starting from the object j. For a generic object k, the two indices are obtained from

$$\text{Influence}(k) = \sum_{j=1}^{N_{\text{tot}}} I(k,j)$$

$$\text{Vulnerability}(k) = \sum_{i=1}^{N_{\text{tot}}} I(i,k).$$

Both these values are shown in Fig. 11.

As one can expect, the influence is very strong among satellites on similar orbits such as the already cited group SC5-SC9 and the group SC1-SC4. SC10 has, instead, the lowest influence because it is in an orbit with lower inclination than the other objects and, therefore, its fragmentations affect a smaller range of latitudes.

A high vulnerability is registered for SC1, which is in a lower orbit than the other spacecraft and which has a much larger cross-sectional area. This explains why it is affected by all the fragmentations originating from the other spacecraft. On the other hand, SC10 is the least vulnerable target because of its high altitude (with more than 115 km of separation between its semi-major axis and the one of the closest object) and because of its small cross-sectional area.

The computational time required to generate Fig. 10 is equal to 645 s on a PC with 8 CPUs at 3.40 GHz. The process is fully automatic and parallized, so the number of spacecraft in the list can

be extended to obtain a more complete picture of the mutual influence among what are considered the most critical objects in the debris population in LEO.

VI. Conclusion

Small debris fragments are often not included in the study of the evolution of the debris population even if they can still pose a relevant hazard to spacecraft in case of collision. The number of small fragments is too large to follow each object separately, so a method to study them in terms of their resulting spatial density was proposed. This requires converting the information on the position of the fragments into a continuous density function. The approach used derives the spatial density from the fragments' orbital parameters and not directly from their positions. It was shown how in this way the results are less dependent on the the run of the breakup model used to produce the fragment cloud. Once the initial density profile was defined, its evolution with time under the effect of drag was obtained by applying the continuity equation, which allows deriving an explicit expression for the density as a function of time and distance. The dependence of the fragment density on the latitude was instead neglected as the focus was on the long term evolution of the cloud, whereas the latitude of a possible target spacecraft evolves on a much shorter time scale. The explicit expression for the density allows the method to provide a very fast estimation of the extension of the region of space affected by the fragmentation and of the resulting collision probability for a spacecraft in that region. For this reason, the proposed method can be applied to simulate many collision scenarios in a short time, enabling new analysis on the contribution of small fragments to the collision probability. In particular, here the method was applied to study the mutual influence among a list of spacecraft in the case they originate a fragment cloud as a result of a small breakup. The resulting matrix of collision probability can be useful to identify which objects, in case of fragmentations, are more likely to have a large effect on the global collision probability and are therefore critical items in the debris population.

Appendix A

The expression of the spatial density can be obtained starting from the hypothesis of mean anomaly M equally distributed. In this case the density $n_M(M)$ will be constant with M and the

follow condition holds

$$\int_0^{2\pi} k\, dM = 1. \tag{27}$$

The first step is to obtain the distribution with the true anomaly ν. Starting from the definition of M

$$M = E - e \sin E, \tag{28}$$

with E eccentric anomaly, dM can be written as

$$dM = \left(\frac{dE}{d\nu} - e \cos E \frac{dE}{d\nu} \right) d\nu \tag{29}$$

$$= \left[\frac{\sqrt{1-e^2}}{1+e\cos\nu} - e \frac{e+\cos\nu}{1+e\cos\nu} \frac{\sqrt{1-e^2}}{1+e\cos\nu} \right] d\nu \tag{30}$$

$$= \frac{(1-e^2)^{\frac{3}{2}}}{(1+e\cos\nu)^2} d\nu. \tag{31}$$

Therefore,

$$n_\nu(\nu) = \frac{(1-e^2)^{\frac{3}{2}}}{(1+e\cos\nu)^2} \tag{32}$$

which is identical to the expression by McInnes and Colombo [34], beside a constant term due to the different choice in the normalization.

The following step is the translation into a distribution in r. Starting from the definition of r the expression for $d\nu$ is found.

$$r = \frac{a(1-e^2)}{1+e\cos\nu} \quad \Rightarrow \quad dr = \frac{a(1-e^2)}{(1+e\cos\nu)^2} e \sin\nu\, d\nu \tag{33}$$

It is convenient to express $\sin\nu$ as

$$\sin\nu = \sqrt{1-\cos^2\nu} = \sqrt{1 - \frac{1}{e^2}\left[\frac{a}{r}(1-e^2) - 1\right]^2} \tag{34}$$

$$= \sqrt{1-e^2}\frac{a}{er}\sqrt{e^2 - \left(\frac{r}{a} - 1\right)^2} \tag{35}$$

so that

$$d\nu = \frac{(1+e\cos\nu)^2}{(1-e^2)^{\frac{3}{2}}} \frac{r}{a^2} \frac{1}{\sqrt{e^2 - \left(\frac{r}{a}-1\right)^2}}\, dr. \tag{36}$$

Substituting $d\nu$ in

$$\int k \frac{(1-e^2)^{\frac{3}{2}}}{(1+e\cos\nu)^2}\, d\nu \tag{37}$$

one obtains

$$\int k\frac{r}{a^2}\frac{1}{\sqrt{e^2-\left(\frac{r}{a}-1\right)^2}}\,dr \tag{38}$$

so the distribution $n_r(r)$ in r is

$$n_r(r) = k\frac{r}{a^2}\frac{1}{\sqrt{e^2-\left(\frac{r}{a}-1\right)^2}}. \tag{39}$$

Eq. 39 has as dimensions [1/km]; to obtain a real spatial density other two steps are required. Firstly, the number of objects in a bin are counted and secondly, the number is divided by the volume of the shell defined by the altitude bin.

For the first step, a rigorous approach will require

$$N(r;\Delta h) = \int_r^{r+\delta h} k\frac{r}{a^2}\frac{1}{\sqrt{e^2-\left(\frac{r}{a}-1\right)^2}}\,dr; \tag{40}$$

if we consider $\Delta h \to 0$,

$$N(r;\Delta h) = \int_{-\infty}^{r} k\frac{r}{a^2}\frac{1}{\sqrt{e^2-\left(\frac{r}{a}-1\right)^2}}\,dr - \int_{-\infty}^{r+\Delta h} k\frac{r}{a^2}\frac{1}{\sqrt{e^2-\left(\frac{r}{a}-1\right)^2}}\,dr \approx k\frac{r}{a^2}\frac{1}{\sqrt{e^2-\left(\frac{r}{a}-1\right)^2}}\Delta h. \tag{41}$$

Similarly the volume of the shell can be written as

$$V = \frac{4}{3}\pi[(r+\Delta h)^3 - r^3] = \frac{4}{3}\pi[3\Delta h r^2 + O(\Delta h^2)] \approx 4\pi r^2 \Delta h. \tag{42}$$

The spatial density s is finally obtained as

$$s(r) \approx \frac{n_r(r)\Delta h}{4\pi r^2 \Delta h} = \frac{k}{4\pi a^2 r}\frac{1}{\sqrt{e^2-\left(\frac{r}{a}-1\right)^2}}, \tag{43}$$

which is identical to Kessler's [20] and Sykes' [21] expression apart from a constant ($k = 1$ in his expression).

VII. Acknowledgements

Camilla Colombo acknowledges the support received by the Marie Curie grant 302270 (SpaceDebECM - Space Debris Evolution, Collision risk, and Mitigation), within the 7$^{\text{th}}$ European Community Framework Programme. The authors acknowledge the use of the IRIDIS High Performance Computing Facility, and associated support services at the University of Southampton, in the completion of this work. The authors would like to thank the editor and the reviewers for the detailed comments that contributed to improve the quality of the paper.

VIII. References

[1] Chobotov, V., *Orbital mechanics*, AIAA, Reston, 3rd ed., 2002, pp. 301–334.

[2] Klinkrad, H., *Space Debris: Models and Risk Analysis*, Springer Praxis Books, Springer, 2006, pp. 15, 91-103, 120.

[3] Johnson, N., "Orbital debris: the growing threat to space operations," *33rd Annual Guidance and Control Conference*, Breckenridge, CO, 2010, AAS 10-011.

[4] White, A. E. and Lewis, H. G., "The many futures of active debris removal," *Acta Astronautica*, Vol. 95, Feb. 2014, pp. 189–197,
doi:10.1016/j.actaastro.2013.11.009.

[5] Krisko, P. H., "The predicted growth of the low-Earth orbit space debris environment an assessment of future risk for spacecraft," *Proceedings of the Institution of Mechanical Engineers, Part G: Journal of Aerospace Engineering*, Vol. 221, No. 6, Jan. 2007, pp. 975–985,
doi:10.1243/09544100JAERO192.

[6] McKnight, D. S., Di Pentino, F. R., and Knowles, S., "Massive collisions in LEO – A catalyst to initiate ADR," *65th International Astronautical Congress*, Toronto, 2014, IAC-14-A.6.2.1.

[7] Rossi, A., Cordelli, A., Pardini, C., Anselmo, L., and Farinella, P., "Modelling the space debris evolution: Two new computer codes," *Space Flight Mechanics – Advances in the Astronautical Sciences series*, Vol. 89, Univelt, San Diego, April 1995, pp. 1217–1231, AAS 94-157.

[8] McInnes, C. R., "An analytical model for the catastrophic production of orbital debris," *ESA Journal*, Vol. 17, No. 4, 1993, pp. 293–305.

[9] Letizia, F., Colombo, C., and Lewis, H. G., "Analytical model for the propagation of small debris objects clouds after fragmentations," *Journal of Guidance, Control, and Dynamics*, Vol. 38, No. 8, 2015, pp. 1478–1491,
doi:10.2514/1.G000695.

[10] Johnson, N. L. and Krisko, P. H., "NASA's new breakup model of EVOLVE 4.0," *Advances in Space Research*, Vol. 28, No. 9, 2001, pp. 1377–1384,
doi:10.1016/S0273-1177(01)00423-9.

[11] Krisko, P. H., "Proper Implementation of the 1998 NASA Breakup Model," *Orbital Debris Quarterly News*, Vol. 15, No. 4, 2011, pp. 4–5.

[12] McKnight, D. S., "A phased approach to collision hazard analysis," *Advances in Space Research*, Vol. 10, No. 3-4, Jan. 1990, pp. 385–388,
doi:10.1016/0273-1177(90)90374-9.

[13] Jehn, R., "Dispersion of debris clouds from In-orbit fragmentation events," *ESA Journal*, Vol. 15, No. 1, 1991, pp. 63–77.

[14] Colombo, C., "Long-term evolution of highly-elliptical orbits: luni-solar perturbation effects for stability and re-entry," *25th AAS/AIAA Space Flight Mechanics Meeting*, Williamsburg, VA, Jan. 2015, AAS 15-395.

[15] Vallado, D. A., *Fundamentals of astrodynamics and applications*, Springer, 4th ed., 2013, pp. 551–573, 619–688.

[16] King-Hele, D., *Satellite orbits in an atmosphere: theory and application*, Blackie, Glasgow and London, 1987, pp. 44 – 62.

[17] Ashenberg, J., "Formulas for the phase characteristics in the problem of low-Earth-orbital debris," *Journal of Spacecraft and Rockets*, Vol. 31, No. 6, Nov. 1994, pp. 1044–1049, doi:10.2514/3.26556.

[18] Orbital Debris Program Office, "History of On-orbit fragmentations," Jsc 62530, NASA, May 2004.

[19] Letizia, F., Colombo, C., and Lewis, H. G., "Continuity equation method for debris cloud evolution," *Key Topics in Orbit Propagation Applied to SSA*, April 2014.

[20] Kessler, D. J., "Derivation of the collision probability between orbiting objects: the lifetimes of Jupiter's outer moons," *Icarus*, Vol. 48, No. 1, Oct. 1981, pp. 39–48, doi:10.1016/0019-1035(81)90151-2.

[21] Sykes, M., "Zodiacal dust bands: Their relation to asteroid families," *Icarus*, Vol. 9, No. 2, 1990, pp. 267 – 289, doi:10.1016/0019-1035(90)90117-R.

[22] Öpik, E. J., "Collision probabilities with the planets and the distribution of interplanetary matter," Royal Irish Academy, May 1951, pp. 165–199.

[23] Su, S.-Y. and Kessler, D., "Contribution of explosion and future collision fragments to the orbital debris environment," *Advances in Space Research*, Vol. 5, No. 2, Jan. 1985, pp. 25–34, doi:10.1016/0273-1177(85)90384-9.

[24] Kessler, D., "Collision probability at low altitudes resulting from elliptical orbits," *Advances in Space Research*, Vol. 10, No. 3, 1990, pp. 393–396, doi:10.1016/0273-1177(90)90376-B.

[25] Jenkin, A. B. and Gick, R. A., "Dilution of disposal orbit collision risk for the medium earth orbit constellations," *4th European Conference on Space Debris (ESA SP-587)*, edited by D. Danesy, European Space Agency, ESA Publication Division, Noordwijk, Netherlands, 2005, pp. 309–314.

[26] Jenkin, A., "Probability of collision during the early evolution of debris clouds," *Acta Astronautica*, Vol. 38, No. 96, 1996, pp. 525–538,
doi:10.1016/0094-5765(96)00059-8.

[27] Chan, F. K., *Spacecraft collision probability*, Aerospace Press, El Segundo, 2008, Chapter 12, Close Encounters with Multiple Satellites.

[28] Letizia, F., Colombo, C., and Lewis, H. G., "Continuity equation approach for the analysis of the collision risk due to space debris clouds generated by a fragmentation event," *65th International Astronautical Congress*, International Astronautical Federation, Toronto, Sept. 2014, IAC-14.A6.P.31.

[29] Rossi, A., Lewis, H. G., White, A. E., Anselmo, L., Pardini, C., Krag, H., and Bastida Virgili, B., "Analysis of the consequences of fragmentations in Low and Geostationary orbits," *Advances in Space Research*, May 2015,
doi:10.1016/j.asr.2015.05.035.

[30] NASA Orbital Debris Program Office, "Flurry of Small Breakups in First Half of 2014," *Orbital Debris Quaterly News*, Vol. 18, No. 3, 2014, pp. 1–2.

[31] Hanada, T., Liou, J.-C., Nakajima, T., and Stansbery, E., "Outcome of recent satellite impact experiments," *Advances in Space Research*, Vol. 44, No. 5, Sept. 2009, pp. 558–567,
doi:10.1016/j.asr.2009.04.016.

[32] Rossi, A., "NASA Breakup Model Implementation Comparison of results," *24th IADC Meeting*, 2006.

[33] Letizia, F., Colombo, C., and Lewis, H. G., "Small debris fragments contribution to collision probability for spacecraft in Low Earth Orbit," *Space Safety is No Accident, 7th IAASS Conference*, Springer International Publishing, May 2015, pp. 379 – 387.

[34] McInnes, C. R. and Colombo, C., "Wave-like patterns in an elliptical satellite ring," *Journal of Guidance, Control, and Dynamics*, Vol. 36, No. 6, 2013, pp. 1767–1771,
doi:10.2514/1.55956.